Author/s:
Falahatdoost, S;Prawer, YDJ;Peng, D;Chambers, A;Zhan, H;Pope, L;Stacey, A;Ahnood, A;Al Hashem, HN;De León, SE;Garrett, DJ;Fox, K;Clark, MB;Ibbotson, MR;Prawer, S;Tong, W

Title:
Control of Neuronal Survival and Development Using Conductive Diamond

Date:
2024-01-31

Citation:
Falahatdoost, S., Prawer, Y. D. J., Peng, D., Chambers, A., Zhan, H., Pope, L., Stacey, A., Ahnood, A., Al Hashem, H. N., De León, S. E., Garrett, D. J., Fox, K., Clark, M. B., Ibbotson, M. R., Prawer, S. & Tong, W. (2024). Control of Neuronal Survival and Development Using Conductive Diamond. ACS Applied Materials and Interfaces, 16 (4), pp.4361-4374. https://doi.org/10.1021/acsami.3c14680.

Control of Neuronal Survival and Development Using Conductive Diamond

Samira Falahatdoost[1], Yair D. J. Prawer[2], Danli Peng[1], Andre Chambers[1,3], Hualin Zhan[1,5], Leon Pope[6], Alastair Stacey[6], Arman Ahnood[7], Hassan N. Al Hashem[7], Sorel E. De León[7], David J. Garret[7], Kate Fox[7], Michael B. Clark[2], Michael R. Ibbotson[4], Steven Prawer[1], Wei Tong[1,]*

[1] School of Physics, The University of Melbourne, Parkville, Victoria, 3010, Australia

[2] Department of Anatomy and Physiology, The University of Melbourne, Parkville, Victoria, 3010, Australia

[3] Department of Mechanical Engineering, The University of Melbourne, Parkville, Victoria, 3010, Australia

[4] Department of Biomedical Engineering, The University of Melbourne, Melbourne, Victoria, 3010, Australia

[5] School of Engineering, The Australian National University, Canberra, Australian Capital Territory, 2601, Australia

[6] School of Science, STEM College, The RMIT University, Melbourne, Victoria, 3000, Australia

[7] School of Engineering, The RMIT University, Melbourne, Victoria, 3000, Australia

[*] Corresponding author: wei.tong@unimelb.edu.au

KEYWORDS. Conductive diamond, N-UNCD, Near infrared illumination, Neurite outgrowth, Neural engineering

ABSTRACT. This study demonstrates the control of neuronal survival and development using nitrogen-doped ultrananocrystalline diamond (N-UNCD). We highlight the role of N-UNCD in regulating neuronal activity via near-infrared illumination, demonstrating the generation of stable photocurrents that enhance neuronal survival and neurite outgrowth, and foster a more active, synchronised neuronal network. Whole transcriptome RNA sequencing reveals that diamond substrates improve cellular/substrate interaction by upregulating extracellular matrix and gap junction-related genes. Our findings underscore the potential of conductive diamond as a robust and biocompatible platform for non-invasive and effective neural tissue engineering.

1. INTRODUCTION

Techniques that can enhance neurite development and outgrowth hold great potential in tackling both neural injuries and neurodegenerative diseases by fostering neural regeneration

and restoration [1]. Recent years have seen the development of a variety of approaches aiming to modulate neuronal survival and neurite outgrowth via chemical, electrical, and mechanical stimuli [2]. As neurons are electroactive, electrical stimulation has been considered one of the most efficient methods. The therapeutic potential of electrical stimulation has already been demonstrated in the treatment of peripheral nerve injuries, where it promotes and guides neurite outgrowth [3-4].

A range of photoelectric materials have been developed and employed to modulate neural activities by converting light into electrical signals [2, 5]. Compared to direct electrical stimulation, optical stimulation via these photoelectric materials provides several advantages [6]. Firstly, optical stimulation eliminates the need for wires that connect electronic implants with external devices for powering and data transmission. The potential for wireless stimulation simplifies the device design and fabrication, reduces surgical complexity, and decreases the risks of post-surgery infection by eliminating percutaneous connectors. Secondly, in electronic implants, the spatial pattern of electrical stimulation is predefined by the electrode array arrangement, and the electrode density limits its resolution. However, optical stimulation offers higher flexibility and precision; advanced optical instruments allow the delivery of versatile illumination patterns at a high spatiotemporal resolution. Thirdly, many photoelectric materials respond specifically to different illumination wavelengths, which leads to diverse cell/material interactions. Therefore, these photoelectric materials can provide an additional degree of freedom for control of neuronal activities depending on the chosen wavelength and spatial arrangement of the illumination.

Some of the photoelectric materials that have been proposed and employed for controlling neuronal development and neurite outgrowth include silicon [7], conductive polymers such as

poly(3-hexylthiophene-2, 5-diyl) (P3HT) [8-16], and carbon-based materials such as graphene oxide [17-19] and graphitic carbon nitride [20-23]. The favourable neural stimulation effects of these materials under illumination have been demonstrated using various cultured cell models, including pheochromocytoma (PC12) cells [9-10, 20-21], primary cortical neurons [12, 14], and neural stem cells [8, 17-19]. Most of these photosensitive materials generate Faradic currents upon illumination via photo-induced electrons and holes[20-21]. Previous research indicates that the direct transfer of electrons (Faradic charge injection) may have a negative impact on the survival of neurons due to the production of a high level of reactive oxygen species (ROS) [9]. Therefore, additional chemicals, such as ascorbic acid, are required to scavenge the photoexcited holes in the cultures [20-21], which limits their *in vivo* and clinical applications. Therefore, photoelectric materials that do not produce Faradic charge injection are highly desirable. In general, biomedical applications can benefit from using light with longer wavelengths due to their deeper tissue penetration potential and reduced phototoxicity, but most photoelectric materials only respond to visible light. Finally, the long-term stability of the implant materials is an important parameter to be considered when designing biomedical devices. However, the long-term stability of photoelectric materials has rarely been studied and reported [16].

Diamond has been considered a suitable material for many biomedical applications due to its high chemical/biochemical inertness, and durability [24-25]. These biomedical applications have been reviewed [24-26], with *In vitro* applications including cell culture substrates and *in vivo* applications focusing more on implant and prosthesis coatings. The biocompatibility of diamond has been confirmed in many studies [24-25, 27]. For example, the number of human sperm cells with grade A motility was found to increase by ~300% after 1 hour's contact with the nanodiamond coated surface, as compared to polystyrene Petri dishes [27]. Nanostructured diamond has also been shown

to facilitate the growth of cortical neurons [28] and to promote the attachment, proliferation and survival of neural stem cells [29]. Among different types of diamond, nitrogen-doped ultrananocrystalline diamond (N-UNCD) stands out due to its high electrical conductivity, which is a result of nitrogen additives increasing the concentration and thickness of grain boundaries that are mainly composed of sp^2-bonded carbon species [30-31]. Moreover, the surface of N-UNCD can be engineered to exhibit various electrochemical properties [32-35]. The biocompatibility of N-UNCD has been validated both *in vitro* [32] and *in vivo* [36-37]. N-UNCD has already been employed successfully as an electrode material for neural stimulation and recording [38-41], including its application in a high-acuity retinal implant for vision restoration [36, 42].

In our previous work, we explored the photoelectric properties of N-UNCD, highlighting its response not only to visible light wavelengths but also to the near-infrared (NIR) range [33-34, 43]. We observed that under NIR illumination, the photoresponse changes depending on the surface termination [34]. For example, in saline solution, hydrogen-terminated N-UNCD shows an illumination induced Faradaic charge transfer mechanism, while oxygen-terminated N-UNCD electrodes predominantly exhibit capacitive photocurrents. This capacitive charge transfer involves a redistribution of charged chemical species within the electrolyte without any direct charge exchange across the electrode/electrolyte interface [44-45]. Such a capacitive charge transfer is considered safer than the Faradaic charge transfer for biological applications [46]. In a recent study, we demonstrated oxygen annealing as an effective method to enhance the capacitive photoelectric responses of N-UNCD to NIR illumination [33]. Our findings indicated that photoresponses increased proportionally to the annealing duration, reaching a maximum response when heated in oxygen at 420 ºC for 25 hours [33].

In this study, we investigate the use of oxygen-annealed N-UNCD as a robust and effective photoelectric platform for wirelessly modulating neuronal development and neurite outgrowth. To achieve this, we first fabricated oxygen-annealed N-UNCD electrodes with different degrees of photoresponsivity to NIR. We then characterised their surface properties using photo-electrochemistry, X-ray photoelectron spectroscopy (XPS), scanning electron microscopy (SEM) and atomic force microscopy (AFM). Following this, we assessed the long-term stability of their photoresponses under different biological conditions. We then assessed the impact of these materials on neuronal development and neurite outgrowth using primary cortical neuron cultures, as depicted in Schematic 1. Finally, we investigated the effects of substrates and stimuli on the cells via calcium imaging and whole transcriptome RNA sequencing. This approach allowed us to evaluate not just the structural, but also the functional and molecular effects of the oxygen-annealed N-UNCD platform on neuronal development and neurite outgrowth.

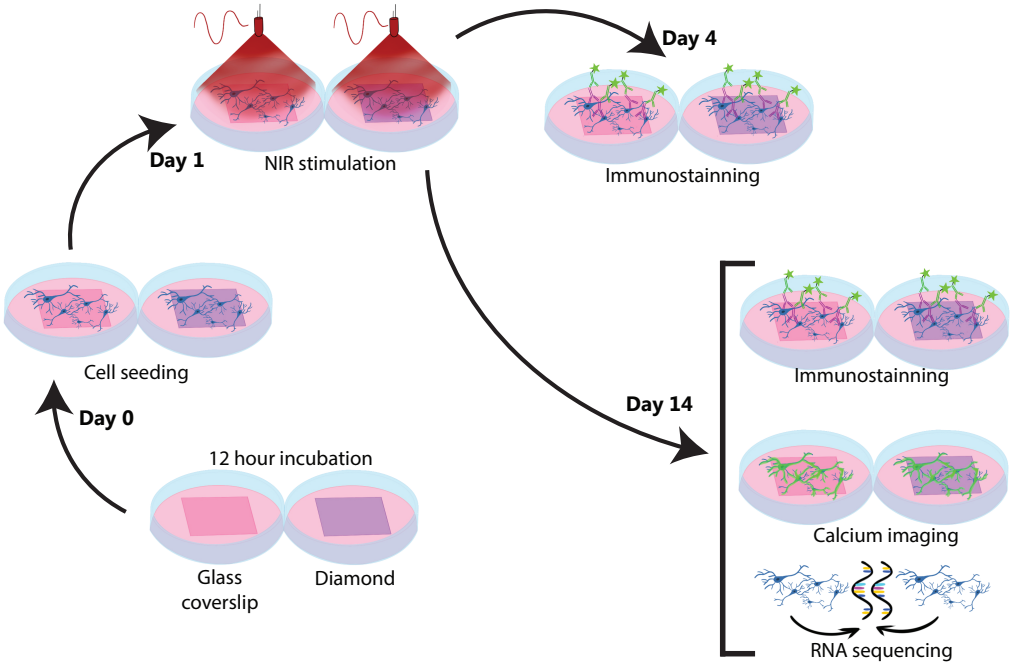

Schematic 1. Methodology Workflow for Studying the Impact of Diamond Substrates and Near-infrared (NIR) Light Exposure on Primary Cortical Neurons. The process began with incubating glass coverslip controls and diamond substrates in Neurobasal-A medium solution for 12 hours. Primary cortical neurons harvested from postnatal rats were seeded onto the samples at a density of 1.4×10^5 cells cm^{-2}. Subsequently, half of the samples from each substrate were exposed to 810 nm NIR light on the first day in vitro (Day 1) at an intensity of 20 mW cm^{-2} and a frequency of 50 mHz, for 16 hours. Cellular structure and morphology of a portion of the cells were assessed on Day 4 via fixation and immunostaining with β-III tubulin and propidium iodide. On Day 14, the assessment was expanded to include not only immunostaining but also calcium imaging and whole transcriptome RNA sequencing. The latter two methods were employed to explore the functional and molecular effects of the substrate and light exposure on the cells.

2. RESULTS

2.1 Diamond Fabrication and Surface Characterization

N-UNCD films were deposited on silicon substrates using microwave plasma-enhanced chemical vapor deposition, as detailed in Experimental Section. Oxygen annealing time affects the electrochemical and surface properties of the N-UNCD samples. We investigated N-UNCD samples after 3 annealing durations: 5, 15, and 25 hours (hereafter denoted 5-hr OA, 15-hr OA, and 25-hr OA, where OA refers to 'oxygen anneal'). Figure 1a shows the photocurrents of the N-UNCD samples measured in the saline solution while pulsing an 808 nm laser at an intensity of 41 mW mm^{-2} and a frequency of 50 mHz. Light with an 808 nm wavelength has been previously

demonstrated capable of penetrating human scalp, skull, meninges and brain, reaching a depth of approximately 40 mm [47]. Compared to the 660 or 940 nm wavelengths, 808 nm showed less absorption and scattering [47]. Consistent with our previous findings [33], the 5-hr OA sample showed a typical capacitive charge transfer in response to pulsed illumination. This is evidenced by a sharp initial peak in the photocurrent followed by a slower decay, with a charge-balanced and biphasic waveform. For samples treated with 15-hr and 25-hr oxygen annealing, we observed photocurrent transients that exhibit both capacitive and Faradaic characteristics. The presence of positive and negative currents in response to the light being turned on and off indicates a predominant capacitive behavior. However, the asymmetry of these currents, combined with the residual current at the end of the positive pulses, suggests the presence of a minor Faradaic current component. This is in line with previous modelling work, which found that both capacitive and Faradaic currents are present for longer annealing times [16]. The amplitude of the peak photocurrent demonstrated an increase in correlation with the annealing duration, ultimately reaching a maximum of 96.15 ± 3.45 μA/ cm^2 in the samples of N-UNCD that underwent a 25-hour annealing process.

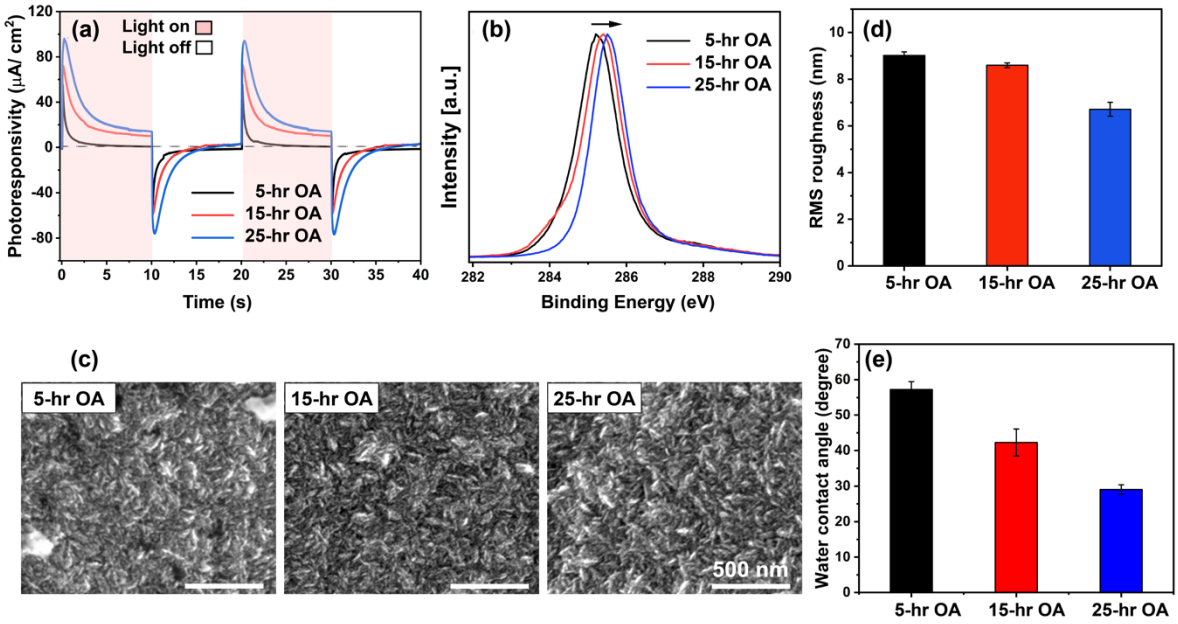

Figure 1. Surface Characterization and Photocurrent Response of Oxygen-Annealed (OA) N-UNCD Samples. (a) Transient photocurrent density of OA N-UNCD samples when subjected to NIR light (808nm, 50 mHz pulse rate, maximum intensity of 41 mW mm^{-2}, and 1.7 mm^2 illumination area). The samples were measured in saline solution, using a 3-electrode setup as detailed in the Experimental Section. The peak photocurrent density increases with annealing duration. (b) XPS high-resolution carbon 1s spectra of N-UNCD samples demonstrate an increase in binding energy with annealing duration, suggesting an increase in oxygen functional groups. (c) SEM images show no significant difference in the surface topography of 5-, 15-, and 25-hr OA samples. (d) Root-mean-square (RMS) roughness as measured using AFM and (e) water contact angle of N-UNCD samples decrease with annealing duration.

We previously suggested that oxygen annealing improved the photoresponse of N-UNCD via a combination of the introduction of oxygen surface functionality and grain boundary etching [33]. In our previous research, we utilised Raman spectroscopy, Near Edge X-Ray Absorption Fine Structure (NEXAFS) measurements, and electrochemical equivalent circuit fitting to elucidate the varying photoresponses of diamond samples [33]. Fig. 1b displays the high-resolution carbon-1s XPS spectra of the N-UNCD samples after different annealing periods. An increase in binding energy indicates that more oxygen functional groups were chemically bonded to the surface when the annealing duration increased [19]. The surface morphology of the N-UNCD samples was expected to change due to a grain boundary etching. The SEM images of the N-UNCD samples are shown in Fig. 1c, which did not show a significant change in surface morphology. However, AFM (Fig. 1d) revealed that the RMS roughness of the surface decreased ~~somewhat~~ with the annealing duration. The oxygen annealing additionally increased the hydrophilicity of the samples, resulting in smaller water contact angles on the samples that underwent a more extensive oxygen annealing duration (Fig 1e).

2.2 Diamond Photoelectrochemical Stability

Electrode stability is important for long-term applications; therefore, we investigated the stability of N-UNCD photoresponse under different conditions. We first compared their photoresponse before and after sterilisation, an essential procedure before using the samples in cell studies (Figs. 2a and c). Sterilisation was conducted using an autoclave which was performed at 134 °C and 235 kPa for 7 min. All the samples showed high stability, with only a less than 6% increase in photocurrents after the autoclave treatment. We then incubated the autoclaved samples for 3 weeks in a culture medium containing 15% horse serum at 37 °C, and 5% CO_2. This horse

serum-supplemented culture medium has been used previously to mimic physiological conditions [48]. It is therefore used here to investigate the possible effect of proteins in solution on the surface termination and photoresponse. The photocurrent remained stable on the 5-hr OA and 15-hr OA N-UNCD samples but dropped 10.7% for the 25-hr OA N-UNCD samples. The shape of the transient photocurrent curve did not change and stayed stable (Fig. 2c).

The stability of the electrodes was further demonstrated by measuring the photoresponse after repetitive laser pulses. Fig. 2b summarises the change of photocurrents after the samples were exposed to over 3000 pulses at a frequency of 50 mHz, for a total of 16.5 hours. The illumination was at an intensity of 41 mW mm^{-2}. The measurement was repeated every 150 pulses, and the peak photocurrents showed less than 7% fluctuation in all the samples but remained relatively stable across the testing regime. The transient traces from one 15-hr N-UNCD sample after different pulses are shown in Fig. 2d, illustrating the stability of this sample after a long period of pulsing.

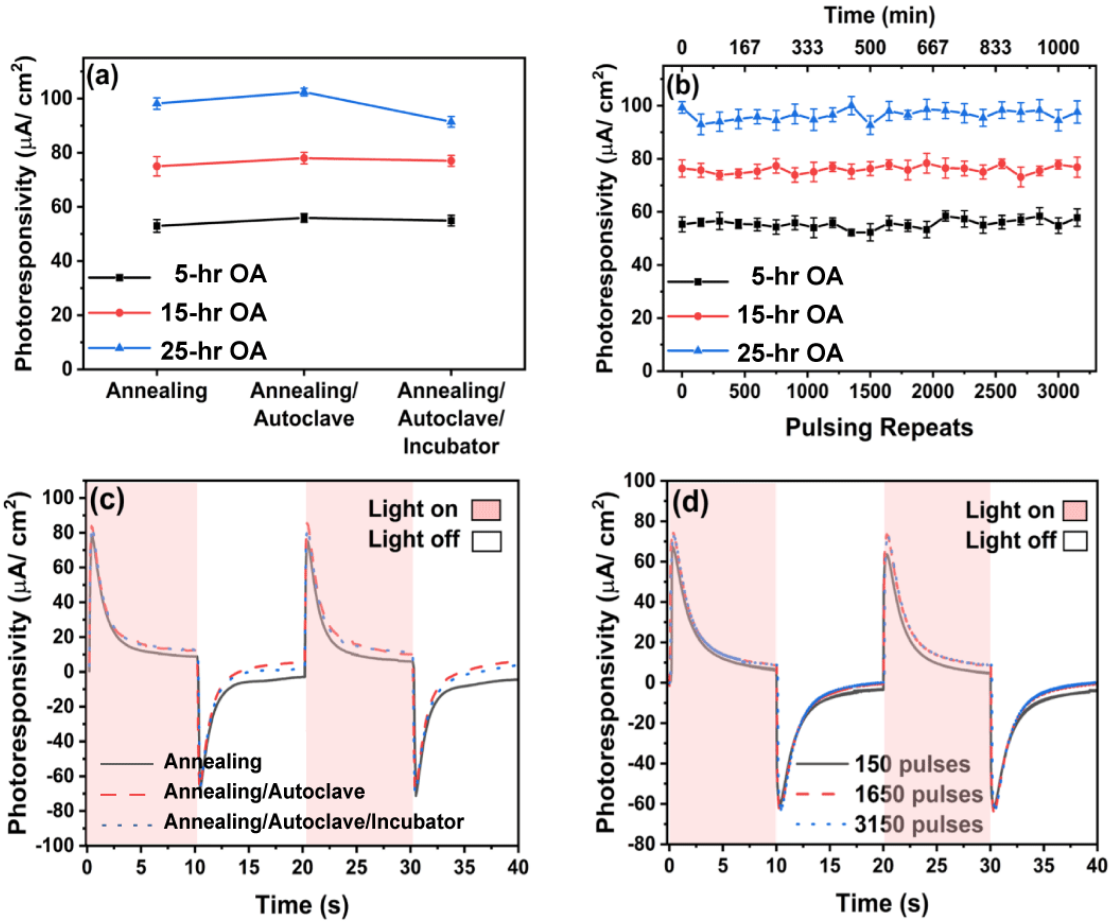

Figure 2. Stability of N-UNCD Photoresponse. (a) Photocurrent comparison for N-UNCD electrode before and after autoclave treatment and three weeks of incubation in a cell culture medium supplemented with 15% horse serum. (b) N-UNCD electrode photocurrent fluctuations following repeated, pulsed illumination. The pulsing was repeated 3000 times at a frequency of 50 mHz, and the photocurrents were measured every 150 pulses. Error bars in (a) and (b) represent the standard deviations. (c) showcases the transient photoresponse of a 15-hr OA N-UNCD electrode, both pre and post autoclave and incubation process. (d) The 15-hr OA N-UNCD response following exposure to varied pulsed illumination.

2.3 Effect of Diamond and Light Exposure on Neuronal Structures

To evaluate the impact of photoresponse from the N-UNCD electrodes on neuronal cells, we built a cell light exposure device as depicted in Fig. 3a. Primary cortical neurons were harvested from postnatal rats and seeded onto three types of N-UNCD samples placed in 24-well dishes with standard Neurobasal-A medium supplemented with B-27, Glutamax and Penicillin-Streptomycin. We used standard coverslips as the control for comparison. Primary cultures, preferred over immortal neuronal cell lines, are more likely to recapitulate the properties of neuronal cells *in vivo* [49]. Prior to cell seeding, all samples were pre-incubated in the Neurobasal-A medium, as described in the Experimental Section, with no additional layer to promote adhesion. Illumination occurred the day after seeding to avoid confounding effects on cell attachment. Half of the cultures were subjected to overnight exposure to 810 nm LEDs at an intensity of 20 mW cm^{-2} and a frequency of 50 mHz, for a duration of 16 hours. The chosen LED intensity was deemed the maximum level that would not introduce a significant temperature change (within 0.5 ºC).

Following this exposure, the cells were then fixed and immunostained on Day 4 for morphological analysis. The representative images of neurons on different substrates, both with and without NIR exposure, are shown in Fig. 3b. On all sample types, neurons survived, extended neurites and formed dense networks. For each condition, three replicates were conducted, with imaging data collected from a minimum of five random regions from each individual sample. Statistical analysis was performed to further study the survival rate and neurite development by comparing cell density (determined by propidium iodide staining), neuron coverage (quantified as the area percentage represented by β-III tubulin staining), and the number of neurites per neuron (manually enumerated using ImageJ), as illustrated in Fig 3c-f. We also studied the cell condition

on each substrate by determining the proportion of neurons that either remain isolated (cell bodies not in contact) or formed small clusters (two neurons with adjacent cell bodies), as shown in Fig. 3f. This assessment was conducted to investigate the impact of the substrate surface on cell aggregation. Neurons prefer to adhere and spread onto surfaces that offer optimal biochemical and biomechanical cues [50]. Therefore, a higher percentage of single-cell or dual-cell aggregations suggests an advantageous condition, as it indicates the cells' preference to adhere to the substrate over clustering with other cells.

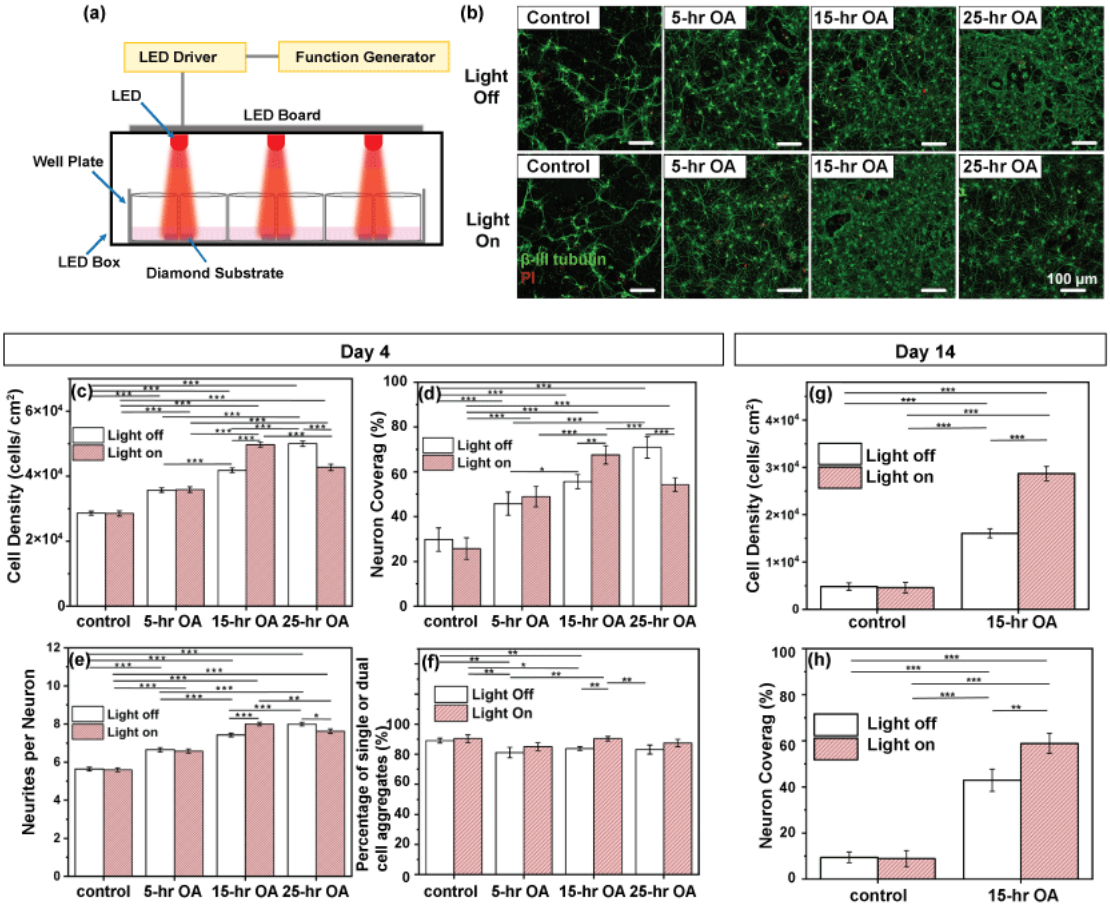

Figure 3. Immunohistochemistry of Cells on Diamond and Control with or without Light Exposure. (a) Diagram of the light exposure setup, comprising a PCB board equipped with six

810 nm LED bulbs, an LED box, an LED driver, and a function generator. A 24-well culture place is shown positioned within the LED box. (b) Representative fluorescent microscope images of neurons at Day 4 on the coverslip controls, as well as the 5-, 15-, and 25-hr OA N-UNCD electrodes with or without NIR stimulation. Neurons were identified by β-III tubulin staining (green), while nuclei are visualised through propidium iodide (PI) staining (red). Quantitative analysis of neuron structures on Day 4 (c-f) and Day 14 (g-h). The graphs show (c,g) cell density (cell/cm^2), (d,h) neuron coverage (quantified as the area percentage represented by β-III tubulin staining), (e) the number of neurites per neuron, and (f) the percentage of single-cell or dual-cell aggregates on the coverslip controls and the OA N-UNCD surfaces under conditions with or without NIR exposure. Error bars represent standard errors. Statistical significance is denoted by $^*p<0.05$, $^{**}p<0.01$, $^{***}p<0.001$.

On Day 4, neurons on all the N-UNCD electrodes exhibited better survival rates compared to those on the coverslip controls. This was evident through the significantly higher cell densities, neuronal coverage, and the increased count of neurites per neuron (Fig. 3c-f). In the absence of light exposure, the survival rates of cells on the N-UNCD samples demonstrated an increase in correlation with the annealing duration (Fig. 3c). This was most noticeable in the 25-hr OA samples, which presented the highest density and coverage of neurons. This result aligns with previous findings [32] and could be attributed to the combined impact of the additional surface oxygen functional groups and changes in surface roughness and hydrophilicity. These aspects will

be discussed in more detail in Section 4. The cell aggregation did not appear to be sensitive to the degree of annealing of the N-UNCD samples (Fig. 3f).

Neurons adhered to the N-UNCD samples and the controls showed remarkably different responses to NIR stimulation (Fig. 3c-f). For neurons adhered to the control coverslips, light exposure had no significant effect on the cell density, neuron coverage, or the number of neurites per neuron, further validating the safety of the light exposure conditions applied in this study. Likewise, the cell survival rate and neurite development on the 5-hr OA samples did not show significant differences upon exposure to light. In contrast, light exposure significantly enhanced cell survival and neurite development on the 15-hr OA surfaces. Following light exposure, the cell density, the neuron coverage, and the number of neurites per neuron on the 15-hr OA electrodes increased by 16%, 18% and 7%, respectively (Fig. 3c-e). Moreover, a larger percentage of single-cell or dual-cell aggregates was observed (Fig. 3f), further affirming the advantageous effect of light exposure on the 15-hr OA samples. Interestingly, light exposure inhibited neuronal survival and development on the neurons adhered to the 25-hr OA samples, leading to a significantly reduced cell density, lower coverage, and fewer neurites. However, the cell clustering condition remained unchanged. The cells on the 15-hr OA samples exposed to light displayed a similar density, coverage, and neurite number to the 25-hr OA samples without light exposure. Still, the aggregation analysis (Fig. 3f) revealed that cells exhibited a preference for the former condition, tending to refrain from forming large aggregates.

Upon validating the beneficial impact of the photoresponse from the 15-hr OA samples using short-term cultures (4 days), we extended our investigation to analyse the properties of the neurons after a longer culture period (2 weeks). We examined the morphology of the neurons via immunostaining to evaluate the survival rate of the cultures on Day 14 (Fig. 3g-h). Consistent with

the short-term culture findings, cells survived better on the 15-hr OA samples compared to the coverslip controls, demonstrated by a significantly higher cell density and neuron coverage. NIR exposure further enhanced the survival rate and neurite development on the 15-hr OA samples, but not on the coverslip controls. The cell density on the 15-hr OA samples increased by 1.4 times, and the neuron coverage increased by 27% as a result of light exposure.

2.4 Probing Calcium Activities in Response to Diamond and Light Exposure

We investigated the intracellular calcium activities and their neuronal network properties under different conditions via calcium imaging on Day 14. Fig. 4a shows an image of neurons loaded with calcium indicator Fluo-4 AM, on a 15-hr OA N-UNCD sample following light exposure on Day 14. These labelled neurons exhibited spontaneous activities with corresponding calcium transients shown in Fig. 4b. The fluorescence changes, $\Delta F/F_0$, of individual ROIs were analyzed using CALIMA software, allowing for the identification of calcium spikes. The representative images and recordings of neurons loaded with Fluo-4 AM on different substrrates are shown in Fig. S1 and Video S1, respectively. Each spike displayed an onset due to neuronal activation, followed by a decay back to the baseline, and that corresponded to the slow unbinding rate of calcium ions from the fluorescent probe. Therefore, each peak in the traces represented a single or a burst of intracellular calcium activity.

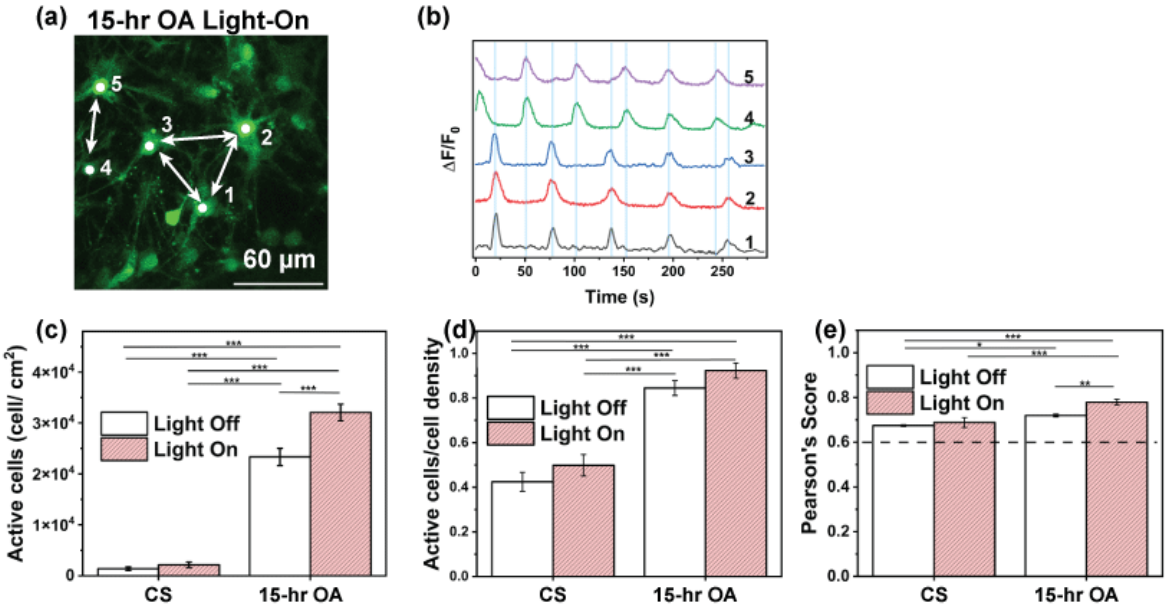

Figure 4. Intracellular Calcium Activity in Neurons on Day 14. (a). Representative images of neurons loaded with Fluo-4 AM on a 15-hr N-UNCD substrate after NIR stimulation on Day 14. The corresponding calcium transients (ΔF/F0 vs. time) of the neurons labelled 1-5 are shown in (b). Connections indicated by arrows were determined via Pearson's cross-correlation analysis. (c) Density of cells exhibiting spontaneous calcium activity. (d) Ratio of spontaneously active cells relative to the total cell count. (e). Pearson's cross-correlation analysis was applied to data collected under various conditions, where a score of 0.6 (dotted line) denotes a high level of cross-correlation. Statistical significance is denoted by $^{*}p<0.05$, $^{**}p<0.01$, $^{***}p<0.001$.

Upon identifying neuronal activities, the analysis proceeded to examine the number of active neurons (Fig. 4c). Given the larger number of surviving neurons on the 15-hr OA samples, the

number of active neurons was significantly higher on these samples compared to the coverslip controls (Fig. 4c). NIR exposure led to a 27% increase in active cell density on 15-hr OA samples. Further analysis of the ratio of active cells to the total number of cells also revealed higher values on the 15-hr OA samples than the coverslip controls (Fig. 4d), but light exposure did not have any significant impact.

Pearson's cross-correlation analysis, facilitated by CALIMA software, was utilized to determine the degree of spatial correlation among neurons exhibiting spontaneous calcium activities. Pearson's algorithm considers the timing of the spikes across ROIs and reports a score between 1 and -1, with 1 symbolising perfect correlation between the distribution signals, a score of -1 representing inverse distribution, and 0 signifying uniform distribution. Pearson's scores, summarised in Fig. 4e, were notably higher on the 15-hr OA samples compared to the coverslip controls. On the N-UNCD samples, light exposure improved the average Pearson's score from 0.7 to nearly 0.8, implying enhanced rhythmic activities in the neurons and a more mature neuronal network. This observation aligns with the morphology findings in Fig. 3g-h, which revealed higher connectivity.

2.5 Transcriptional Profile Changes Induced by Diamond and Light Exposure

We examined the transcriptomic profiles of cells cultured on both control and 15-hr OA samples, with or without light exposure, on Day 14. RNA sequencing was performed using cells from each condition across three replicates (Figure 5). Using integrated Differential Expression and Pathway (iDEP) analysis [51], we first performed a principle component analysis to investigate similarities between gene expression profiles across various samples, as represented in Fig. 5a-b. Notably, the transcriptional profile of cells cultured on the 15-hr OA N-UNCD samples clearly diverged from

the control samples and formed a distinct cluster in Fig. 5b. Principal Component 3 (PC3) exhibited a strong correlation with the substrate type, with a variance value of 13% and a statistically significant p-value of 1.39×10^{-6}. Thus, the N-UNCD substrates lead to changes in the transcriptional profile of neurons that may drive their improved survival and activity.

Next, a differential expression analysis was carried out to identify the quantity of differentially expressed genes across various conditions (Fig. 5c-f). The cut-off threshold for analysis was set at p = 0.05 and Fold Change = 1.5. Fig. 5c summarizes the numbers of differentially expressed genes in each pair and a comprehensive list of the differentially expressed genes can be found in Table S1. We identified more differentially expressed genes when comparing 15-hr OA to control samples without light exposure, than between light-on and light-off conditions, regardless of substrate type. This suggests that the substrate type had a more significant impact than light exposure on the transcriptional responses of the cells.

In comparison to control samples without light exposure, the diamond substrate significantly upregulated several genes related to critical neuronal functions (Fig. 5d). These genes include Gjb6 and Gjb2, which are associated with gap junction proteins [52-53]. Gap junctions provide critical pathways for the propagation of presynaptic electrical currents to postsynaptic sites in neurons, thereby playing a vital role in signal transmission [54]. Additionally, diamond substrates induced the differential expression of genes involved in sodium channel activities, including Slc22a6, Slc6a13, Scn7a, Scl30a3, Slc22a3, and Slc25a34. The collective activity of these genes could potentially facilitate a more active neuronal network on the diamond, as supported by our calcium imaging experiments (Fig. 4). Diamond substrates were also observed to upregulate genes involved in cell attachment, including Cdh5, a gene encoding calcium-dependent cell adhesion molecule[55], and

Col13a1, associated with collagen production[56]. Collagen, an extracellular matrix component, is known to regulate neuronal attachment and signal transduction[57].

Focusing on the differentially regulated genes, we performed a Gene Ontology (GO) enrichment analysis using iDEP [51]. The GO terms that reached statistical significance and ranked in the top 10 are listed in Fig. 5g and Table S2, and are categorised into three classifications: biological process, cellular component, and molecular function. Since gap junction genes, Gjb2 and Gjb6, were significantly upregulated on diamond compared to control samples, they resulted in the enhancement of gap junction-mediated intercellular transport in the biological process category (Table S2). Similarly, "gap junction channel activity involved in cell communication by electrical coupling" was enriched within the molecular function category. These genes led to the upregulation of the connexin complex, a critical element in forming gap junctions. Extracellular space was the most significantly upregulated GO cellular component term, suggesting that diamond may enhance interactions with the cells via the extracellular matrix. Furthermore, genes such as Col13a1 and Cdh5 also induced the upregulation of several substrate-binding processes. These processes potentially contribute to improved cell adhesion and survival on diamond substrates.

When studying the effects of light exposure, Fosb emerged as the only differentially expressed gene on both the control and 15-hr OA samples due to light exposure (Fig. 5e-f). Significant GO terms ($p=0.01$) resulting from light exposure are summarised in Fig. S2 and Tables S3,4. For the control samples, no GO signals pertinent to neuronal health and behaviour emerged. Comparing light-on and light-off conditions on the diamond samples at Day 14, only 10 genes were differentially expressed, suggesting that GO enrichment analysis may not provide reliable insights. Nevertheless, the higher number of significant GO terms observed in diamond samples might

indicate a more specific and directed effect of light exposure on cells when coupled with diamond substrates.

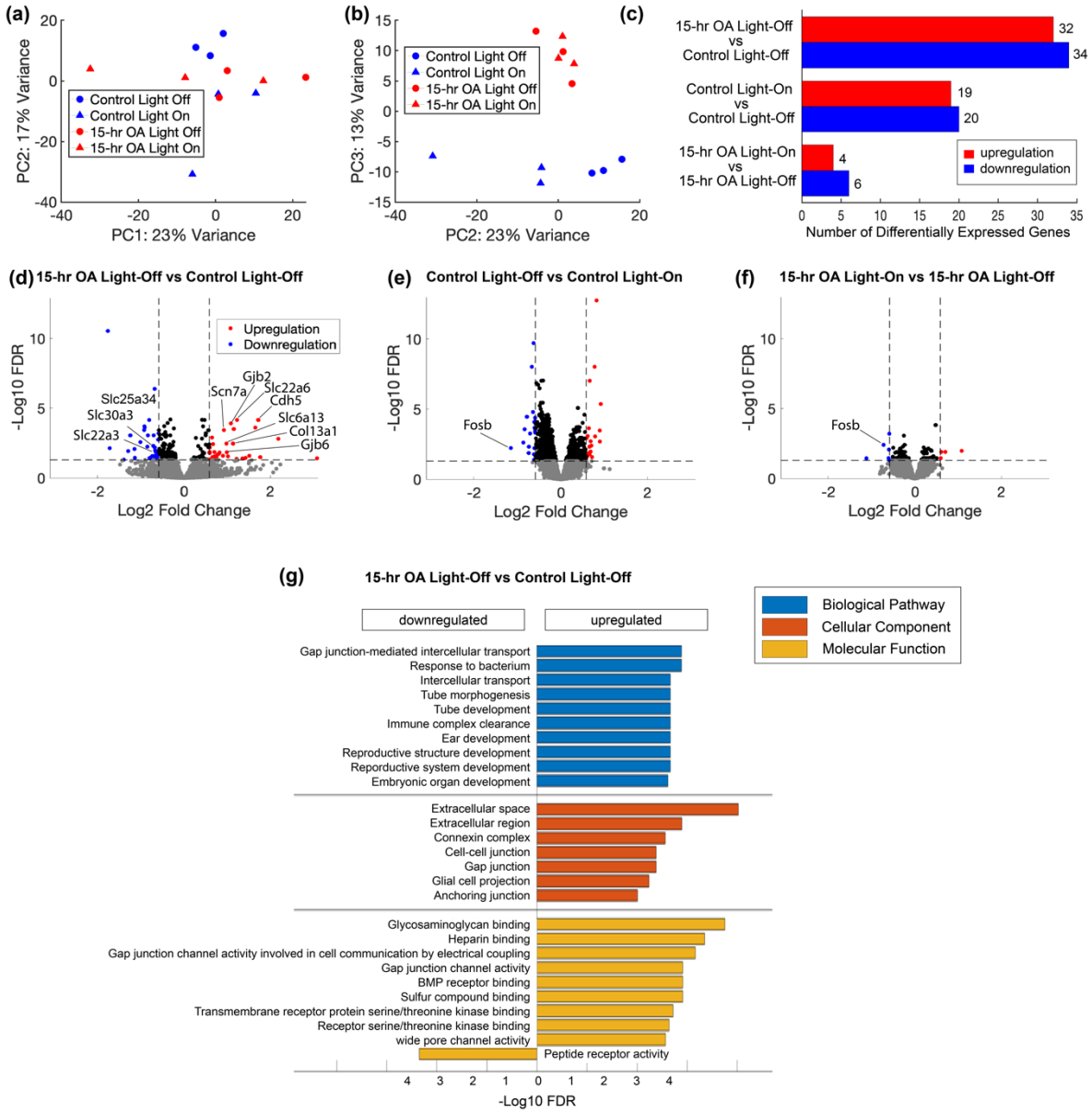

Figure 5. Comparative Analysis of Transcriptional Profiles in Neurons on Day 14. (a,b). Principal component analysis highlighting the variation in gene expression across different conditions, where PC3 exhibits a strong correlation with substrate type ($p=1.39\times10^{-6}$). (c). A

comprehensive summary of differentially expressed genes among different conditions. (d-f) Volcano plot illustrating gene expression, with dotted lines representing the cut-off threshold for analysis (p=0.05, Fold Change=1.5). (g) Gene Ontology (GO) enrichment analysis: the bar charts display upregulated (right) and downregulated (left) GO terms in the respective conditions.

3. DISCUSSION

3.1 Substrate Impact

In this work, we engineered N-UNCD electrodes demonstrating different levels of photoelectric effects and investigated the response of neurons attached to these surfaces when exposed to NIR light. Consistent with our previous findings, all N-UNCD samples displayed a predominantly capacitive photoresponse to NIR stimulation. An increase in oxygen annealing time led to enhanced photoresponsivity in N-UNCD electrodes, which is likely due to an increase in surface oxygen functional groups (Fig. 1b) and the etch of grain boundaries (Fig. 1d). Our photoelectrochemical stability (Fig. 2) showed that all the samples remained highly stable under a variety of biologically relevant conditions. This indicates their potential suitability for robust, long-term biomedical applications.

Our study showed that neurons survived better on N-UNCD electrodes, regardless of the annealing duration, when compared to the coverslip controls, as shown in Fig. 3. These results further confirmed the biocompatibility of N-UNCD. Previous studies have consistently shown diamond to be superior to other routinely used substrates for *in vitro* cell cultures [24-25]. For example, macrophages cultured on diamond were found to down-regulate inflammatory cytokines compared to tissue culture polystyrene (TCP) [58], suggesting that diamond implants may induce a less severe

immune response. Various cells such as epithelial, fibroblasts and neural stem cells have also been found to attach and proliferate better on diamond than quartz, glass, and TCP [59-61]. Furthermore, Sommer *et al.* reported a significant increase in the vitality of human sperm cells when in contact with diamond, in contrast to TCP[27].

Among various diamond samples, the 25-hr OA sample was the most effective in enhancing cell survival, with the highest neurite coverage and number of neurites per neuron. Surface properties such as roughness and wettability have been shown to play important roles in neuronal survival and growth. We previously suggested surface roughness as a major factor influencing neuronal growth on diamond [32]. The role of topography in neurite outgrowth has been demonstrated on different materials, as neurite initiation requires a certain amount of physical space for the proper orientation of cytoskeletal filaments to sprout new processes [62]. The 25-hr OA N-UNCD samples, characterised by the lowest surface roughness (Fig. 1d), may enhance neuronal adhesion and neurite outgrowth by facilitating cellular interactions. Furthermore, the additional oxygen functional groups on the 25-hr OA N-UNCD surface created a more hydrophilic surface, as confirmed by the water contact angle measurements (Fig. 1e). Hydrophilic surfaces tend to promote better cell adhesion, which is critical for neuronal survival and growth. These types of surfaces allow for stronger interactions between the surface and the extracellular matrix proteins, which in turn facilitate cell attachment [63]. The extracellular environment *in vivo* is generally hydrophilic due to the presence of water and polar molecules. Therefore, culturing neurons on hydrophilic surfaces more closely mimics their natural environment, potentially leading to better cell behaviour and functionality.

In this work, we conducted RNA sequencing to compare the transcriptome profiles of cells adhered to coverslip controls and the 15-hr OA samples. To our knowledge, this is the first study

examining the transcriptome profile of neurons adhered to diamond substrates. Our results highlight differences in gene expressions between cells on these two types of materials, i.e. diamond and coverslip, which in turn provides insights into the potential underlying mechanisms. Diamond substrates seemingly enhance cell survival by upregulating genes associated with extracellular matrix production, such as Col13a1 and Cdh5, thereby improving cellular adhesion and viability.

In addition to a higher survival rate, our calcium imaging results suggest that diamond substrates foster a larger proportion of spontaneously active neurons and a higher level of synchronised neuronal activities (Fig. 4). This observation could be attributed to the upregulation of gap junction protein genes, Gjb6 and Gjb2. Gap junctions play critical roles in signal transmission between neurons by controlling the plastic properties of electrical synapses [64]. However, the influence of biomaterials on gap junction formation remains an understudied area. Our findings suggest that further exploration of gap junctions may shed light on the interplay between biomaterials and cells.

3.2 Light Exposure Impact

Low-intensity red or near-infrared light, has been used as a therapeutic approach to stimulate, heal, regenerate and protect injured or degenerated tissues[65]. This therapeutical approach, also known as photobiomodulation was initially primarily studied for stimulation of wound healing, but its beneficial impacts have been found useful in treating brain disorders as well. However, the precise cellular mechanisms underpinning photobiomodulation are not yet fully understood. Known effects of red or near-infrared light include its absorption by cytochrome C oxide and other molecules, which stimulates ATP synthesis and affects ROS production[65]. In our study, we did not notice any significant impact of 810 nm illumination on the structure and calcium activities of

neurons adhered to coverslip controls. The RNA sequencing study revealed ~~some~~ differentially expressed genes in cells on coverslip controls with or without light exposure, but there was no enrichment for pathways clearly related to neuronal health or survival. This indicates that the impact of light exposure on cells on control samples is not highly specific, implying that the effect observed may not be attributed to a well-defined biological process or pathway. However, it is well-established that cells may react differently to light depending on the dose and frequency.

The effects of light stimulation have been published on cells adhered to various photoelectric materials [5-14, 17-23]. Most previous studies used a single material, only examined cellular responses to one level of stimulation, and only reported the favourable effects of light exposure on cells [9-10, 14, 17-21]. By applying different surface treatments to N-UNCD, we were able to examine the cellular response to varying magnitudes of photocurrent and their mechanisms. We generally observed that the 15-hr OA N-UNCD sample produced the most beneficial effect on cells. This could be attributed to a combination of factors. First of all, the 15-hr OA sample exhibited a greater capacitive photoresponse than the 5-hr OA sample, which is expected to produce a greater membrane depolarisation in the cells. Therefore, the illumination only showed beneficial effects on cells adhered to samples with a medium level of photocurrents (15-hr N-UNCD), and had negligible influence when the photocurrent was small (5-hr N-UNCD). On the other hand, although the 25-hr OA N-UNCD sample displayed an even higher photoresponse, it also produced a greater proportion of Faradaic photocurrent. This Faradaic photocurrent is known to cause adverse effects in cells [66] and the overdose of photocurrents from 25-hr N-UNCD negatively impacted neuronal survival and neurite outgrowth. Since illumination did not influence neuronal growth on the coverslip controls, the observed effects on illuminated N-UNCD substrates were mostly attributed to the excitation of the photoactive material. This finding aligns with previous

research, which demonstrated varying cellular responses to electrical stimulation under different charge injection magnitudes [2]. For example, Liu et al showed that a charge injection of 0.08 μC, in a range of 0.01-0.4 μC, elicited the strongest osteogenetic response in osteoblast precursor MC3T3-E1 cells [67]. Our results provide evidence that different levels of capacitive and Faradaic photocurrents from N-UNCD electrodes can be used to regulate neuronal survival and development.

In this study, we selected an illumination intensity that minimally raised the temperature of culture medium by less than 0.5 °C to mitigate potential photothermal effects. However, localised photothermal effects on the substrate surface might occur, which would not be reflected in the overall medium temperature. Further investigations are necessary to discern and quantify the specific contributions of photothermal and photoelectric effects of the substrates on cell cultures.

Here, we studied the intracellular Ca^{2+} activities of neurons on the 15-hr OA N-UNCD substrates and coverslip controls after two weeks of culture. The application of light stimulation induced more spontaneously Ca^{2+} active cells on 15-hr N-UNCD samples. Previous studies have demonstrated the crucial role of intracellular Ca^{2+} activities in cellular response to photoelectrical stimulation [8, 10, 14-15, 22]. For example, Wu *et al.* reported that photostimulation using P3HT nanoparticles could elevate Ca^{2+} levels and increase the expression of L-type voltage-gated calcium channels (L-VGCC) in bone marrow mesenchymal stem cells (BMSCs) [14]. They further confirmed the significance of Ca^{2+} by showing that calcium inhibitor $GdCl_3$ could inhibit the effects of photostimulation on neuronal differentiation of BMSCs.

Contrary to expectations based on previous studies, our RNA sequencing analysis did not reveal significant changes in the expressions of L-VGCC related genes in cells on the 15-hr OA N-UNCD samples after light exposure. This suggests that the different behaviour observed in neurons on the

diamond substrate, with and without light exposure, might be attributed to a different mechanism. This hypothesis is further supported by prior research which investigated the combined effect of light illumination and diamond on sperm cells. The study found that 670 nm LED illumination enhanced the motility of sperm cells on nanodiamond surfaces.[27] with light exposure suggested to increase ATP levels in cells while the nanodiamond surface functioned as a scavenger for the harmful ROSs triggered by light exposure. Similarly, our findings provide a hint, though tentative, that light exposure may downregulate cellular responses to oxygen-containing compounds (Fig. S2). This could, in theory, make cells less susceptible to ROS stimulation, but additional research is needed to confirm this possibility.

3.3 Limitations

This study has several limitations, which can be addressed in future research. Firstly, our study has yet to comprehensively investigate stimulation parameters such as illumination time, frequency, and wavelength. Our initial studies only illuminated cells overnight. Future work will expand the parameter space seeking more precise control over neuronal survival and development. Secondly, while we have provided some insights into the mechanism of how diamond and photoelectrical stimulation modulates neuronal behavior, the exact mechanism remains unclear. Other molecular tools and sequencing strategies could uncover more genes and pathways involved. In this study, the light exposure was conducted on Day 2, and our RNA sequencing experiments were performed on cells at Day 14. This means that our experimental design may not have captured transient cellular responses to both light exposure and the substrate. This is supported by our observation that the benefits of both diamond and photoelectrical stimulation were present by Day 14. Future experiments could involve the monitoring of the transcriptome profile of the cells

across different time points, to better understand how these variables interact. In addition, it is also possible that the beneficial molecular impact of light is at least mediated partially through non-transcriptional mechanisms, as identified previously [14]. These mechanisms could potentially be elucidated through techniques such as reverse transcription polymerase chain reaction (RT-PCR) to analyze gene expression and western blotting to assess specific protein expression. Thirdly, the present work was performed using cultured cells *in vitro*. Therefore, the practical applications of this platform include the use of N-UNCD as a substrate for *in vitro* neuronal cultures, coupled with NIR illumination to expedite culture maturation. Translating these findings to *in vivo* and eventual clinical use will require additional research. N-UNCD films can be applied free-standing by etching away the silicon substrates or used as coatings on other materials or devices [32]. The safety of N-UNCD for chronic applications has been previously demonstrated by implanting N-UNCD adjacent to the retina tissue [36]. As such, a potential application of our findings could involve the use of N-UNCD electrodes in retinal implants, alongside NIR stimulation, to slow down or rescue the degeneration of neurons in retinal diseases, such as retinitis pigmentosa and age-related macular degeneration.

4. CONCLUSIONS

This work reports, for the first time, the use of photoelectric conductive diamond to modulate neuronal survival and outgrowth, thereby providing a potential platform for neural regeneration. N-UNCD films, after oxygen annealing, can generate varying levels of photocurrents in response to NIR stimulation. The photoresponse showed remarkable stability under various biological conditions. Our results showed that N-UNCD surfaces promoted neuronal growth without the need for additional promotive substances, supporting its biocompatibility. Furthermore, the amplitude of the photocurrent under NIR stimulation was found to differentially regulate neuronal survival

and development. This research enabled the development of a biocompatible, nanostructured, and light-sensitive platform that can modulate neuronal survival and development in a wireless, repeatable, and non-invasive manner, without requiring genetic modification. These results suggest great promise for the future application of N-UNCD in long-term, non-invasive neural regeneration.

5. EXPERIMENTAL SECTION

5.1 Diamond Preparation

The N-UNCD films used in this work were fabricated on silicon substrates (n+-doped, 1000 μm thick, single-side polished) using an IPLAS microwave plasma-assisted chemical vapour deposition system, as described in our previous work [35]. Briefly, silicon substrates were first seeded with positively charged 4-6 nm nanodiamonds. Over the course of a three-day CVD growth, we maintained a gas mixture consisting of 79% argon, 20% nitrogen, and 1% methane (*BOC Australia*, purity 99.999%). The microwave power was held at 1000 W, with a stage temperature at 850 °C, and a gas pressure at 80 Torr. The resultant thickness of the N-UNCD films was approximately 32 μm as estimated by *FIE Nova NanoLab 200* SEM. All N-UNCD samples in this study underwent oxygen termination through annealing in an oxygen environment (~0.02 L/min) in a vacuum furnace at 420 °C for 5, 15, or 25 hours, referred to as 5-hr OA, 15-hr OA, and 25-hr OA, where OA denotes 'oxygen anneal'.

5.2 Photoelectrochemical Characterization

The photoresponses of N-UNCD samples to NIR light were studied using photoelectrochemical measurement, as previously described [33]. These experiments were performed in a saline solution (0.15 M NaCl) using a three-electrode electrochemical cell connected to a potentiostat (*Gamry*

Interface 1000E). The three electrode setup consisted of a platinum disk counter electrode, an Ag/AgCl reference electrode (*eDAQ Pty Ltd)*, and the N-UNCD sample serving as the working electrode. For the light source, we used a 0.7 W NIR (808 nm) laser diode (*Wuhan Lilly Electronics*) pulsed with a 10 s on and 10 s off cycle (50 mHz), using a waveform generator (*RIGOL DG4062*). During the characterization, the peak illumination intensity was 41 mW mm^{-2} and the illuminated area was 1.7 mm^2. The photocurrent density was calculated by dividing the peak photocurrent by the illuminated area (1.7 mm^2). Each reported measurement is the average of ten sequential peak photocurrents, and this was done for three samples at each annealing time.

5.3 Surface Chemistry Characterization

X-ray photoelectron spectroscopy (XPS) was used to study the chemical composition of the N-UNCD films. Measurements were carried out on a Thermo-Fisher K-Alpha apparatus using an Al Kα radiation source with E_{photon} = 1486.7 eV.

5.4 Surface Morphology Characterization

The surface morphology and roughness of the N-UNCD films were assessed using Scanning Electron Microscopy (SEM) and Atomic Force Microscopy (AFM). SEM images were acquired using an *FIE Nova NanoLab 200* SEM under the high vacuum mode at 30 kV. AFM topographic maps were obtained using *Asylum MFP-3D AFM* using a Tap300 Al-G tip in the tapping mode. A scanning area of 0.5 × 0.5 μm^2 was selected to capture the changes in the surface morphology over nanoscale lengths.

5.5 Contact Angle Measurement

The sessile-drop contact angle measurements of the 5-hr, 15-hr and 25-hr OA N-UNCD films were measured using a 2.5 μL droplet of Milli-Q water (Merck Millipore, VIC, Australia). This droplet size was selected to prevent the liquid from touching the edges of the samples. The droplet

was carefully placed on the sample surface using a micropipette. Digital images were captured and analysed using a Drop Shape Analyser DSA25 (Kruss GmBH, Hamburg, Germany) at room temperature with a Young Laplace fitting method. The contact angle was acquired 100 times for each drop, and the mean contact angle along with the standard deviation was calculated.

5.6 Stability Tests

The stability of the N-UNCD photoresponses was evaluated via three different tests. Firstly, samples underwent sterilisation using an autoclave before cell seeding, and photoresponses were measured both before and after sterilisation. Autoclaving was performed at 134 °C and 235 kPa for 7 min.

The second test was designed to assess the stability of the electrodes under physiological conditions. This involved monitoring the photoresponses of the N-UNCD films over time while they were incubated in a cell culture medium supplemented with 15% horse serum. The medium comprised Neurobasal A with 2% B-27 supplement (Gibco), 2 mM Glutamax (Gibco), and 100 mg/mL penicillin-streptomycin (Gibco). The incubation conditions were maintained at 37 ^{o}C, 5% CO_2, for a three-week period [48].

Lastly, a third test was conducted to evaluate the stability of the electrodes under conditions of repetitive illumination. The samples were exposed to a pulsed NIR laser operating at 50 mHz with a 10 s on and 10 s off cycle. The peak intensity of the illumination was 41 mW mm^{-2} over 3000 pulses (equivalent to a total duration of 16.5 hours). Photoresponses were measured after every 150 pulses.

5.7 Cell Culture

All cell culture procedures were performed in compliance with the guidelines of the National Health and Medical Research Council of Australia (Australian Code for the Care and Use of

Animals for Scientific Purposes) and approved by the Animal Ethics and Welfare Committee of the University of Melbourne (Ethics ID 1814396).

The N-UNCD films and coverslip controls were sterilised via autoclaving and then placed in 24-well dishes for cell culture experiments, with three replicates for each experimental condition. Before cell seeding, all samples were incubated in the Neurobasal A medium (Gibco) for at least 24 hours without additional coatings.

Primary cortical neurons were harvested by isolating the cerebral cortices from P0-P1 rat pups, as previously described [32]. Briefly, the animals were decapitated, and the heads were immersed in Hank's balanced salt solution (HBSS; Gibco). After removing the skin and skull, a small section of the cortex was taken off using fine forceps. The meninges were then removed, and the tissue was dissected using scalpel blades and collected. The neurons were obtained from the dissociated tissue by protease digestion for 20 minutes at 37 ^{o}C in HBSS containing 10 μg/mL DNase I (Sigma) and 250 mg/mL trypsin (Sigma). Soybean Trypsin Inhibitor (Sigma) containing 10 μg/mL DNase I was used to stop trypsinization. Neurons were centrifuged and then triturated using a P1000 pipette. A cell culture medium containing Neurobasal A with 2% B-27 supplement (Gibco), 2 mM Glutamax (Gibco), and 100 mg/mL penicillin-streptomycin (Gibco) was used to dilute the triturated cells. The cells were seeded at a density of 1.8×10^5 cells/well on both diamond films and control samples. Finally, the cultured primary cortical neural cells were incubated at 37 °C in a 5% CO_2 environment. The culture medium was changed on the second day (Day 2) and then twice weekly thereafter.

5.8 Cell Culture Light Exposure

Half of the samples were exposed to NIR on Day 2 for a duration of 16 hours. During the illumination process, the 24-well dish was placed in a custom-built box, and a board fitted with six

810 nm LEDs (OSLUX®, SFH 4780S) was situated above the dish (Fig. 3a). The LEDs were driven using *a GW Instek GPS-1850D power supply* and pulsed using a waveform generator (*RIGOL DG4062*) at 50 mHz with a 10 s on and 10 s off cycle. All samples were subjected to a peak intensity of 20 mW cm^{-2} as measured using a laser power meter (Coherent, Fieldmax). A fan was attached to the LED board to improve heat dissipation. The temperature change monitored during the light exposure was noted to be less than 0.5 °C.

5.9 Fixation, Immunostaining and Imaging

The cellular morphology was assessed on Day 4 and Day 14 through a process of fixation and immunostaining. The samples were fixed in 4% paraformaldehyde solution for 10 min, then in cold (-20 °C) methanol for 10 minutes and followed by a triple rinse in phosphate-buffered saline (PBS). Subsequently, the samples were incubated for 20 min with a primary antibody solution (mouse anti-β-III tubulin; Promega) after a 30 min pre-treatment with a blocking solution containing 2% fetal calf serum and 2% normal goat serum in PBS. Post-incubation, the films were once again rinsed with PBS and then incubated with secondary antibody (Cy3-conjugated goat anti-mouse immunoglobulin; Jackson Immunolabs) and Propidium Iodide (PI, Sigma-Aldrich) for another 20 min. Finally, the samples were thoroughly rinsed with PBS three times and then stored at 4 °C prior to imaging. Random regions of 636× 636 μm^2 were selected from each sample and imaged using a confocal microscope (Olympus, FV1200) with excitation lasers at 473 nm and 543 nm through a Nikon Plan Apo 0.75-numerical aperture (NA) 20× objective. Images were then analysed using Fiji (ImageJ) [68], MATLAB R2020b and OriginPro 2021.

5.10 Calcium Imaging

To study the electrophysiological properties of the cells, calcium imaging was performed on the 15-hr OA and control samples on Day 14. On the day of imaging, the cultured cells were washed

with PBS and then incubated at 37 °C with a solution containing 5 μM Fluo-4 AM (Invitrogen) in Ames' medium (Sigma) for 20 min. Following this, the samples were transferred under an upright confocal microscope (Olympus, FV1200) for imaging. To maintain physiological conditions during the imaging process, the cells were continuously perfused with carbonated Ames' solution at a flow rate of 3 to 8 ml/min at room temperature. Images were taken using a Nikon Plan Apo 40× objective (0.8 NA), with a laser of excitation wavelength of 473 nm. At least five different regions from each sample were imaged, each with a field of view of 159 × 159 μm^2. The images were captured at a frame rate of 4.8 Hz for a total duration of 3 minutes.

Calcium imaging data was processed using the semi-automated open-source Ca^{2+} imaging analyser CALIMA according to its instructions [69]. This software determined the regions of interest (ROI) and the fluorescence changes in ROIs were normalised to the baseline ($\Delta F/F_0$) and then analysed. Calcium spikes were detected by setting a threshold and the connections between pairs of neurons were determined via the Pearson cross-correlation analysis. Data were analysed further using MATLAB R2022b and OriginPro 2021.

5.11 RNA Sequencing

On Day 14, cells from 15-hr OA and controls were lysed, and their total RNA was extracted in accordance with the manufacturer's instructions using the Qiagen RNeasy Lipid Tissue Mini kit (Qiagen, 74804). PolyA purification, library preparation and 150bp paired end Illumina whole transcriptome sequencing were performed by the Australian Genome Research Facility to a depth of 50 million reads per sample on the NovaSeq platform. Each sample was assigned a unique barcode. Following sequencing, the acquired sequence reads were aligned against a reference genome library using the Spliced Transcripts Alignment to a Reference (STAR) (version 2.3.5a)

[70]. The chosen reference was Rattus norvegicus from NCBI RefSeq version 6, with the accession number GCF_000001895.5. Subsequently, the counts of aligned sequences were analyzed using integrated Differential Expression and Pathway (iDEP) analysis [51]. We first performed a Principal Component Analysis to compare the similarity between cells under different conditions. Following this, differentially expressed genes (DEGs) were identified using the DESeq2 method, with a False Discovery Rate (FDR) cutoff set at 0.05 and a minimum fold change of 1.5. Subsequently, an enrichment pathway analysis in DEGs for each selected comparison was carried out according to the Gene Ontology (GO) categories: biological process, cellular component, and molecular function, using an FDR at 0.01. The results were then exported from iDEP and replotted for clearer visualisation and interpretation using MATLAB R2022b.

5.12 Statistical Analysis

Statistical analysis was performed using IBM SPSS Statistics 27. One-way analysis of variance (ANOVA) or two-way ANOVAs with post-hoc Tukey's tests were performed for multiple comparisons. Data were expressed as mean ± SEM, and $p < 0.05$ was considered statistically significant.

ASSOCIATED CONTENT.

The following file is available free of charge:

- Figure S1: Experimental results of neurons loaded with calcium indicator, Fluo-4 AM, on various substrates; Figure S2: Experimental results of Gene Ontology enrichment analysis; Table S1: A summary of differentially expressed genes under each condition; Table S2: Results of Gene Ontology Enrichment Analysis of 15-hr OA Light-Off vs Control Light-Off; Table S3: Results of Gene Ontology Enrichment Analysis of Control Light-On vs Control Light-Off; Table S4: Results of Gene Ontology Enrichment Analysis of 15-hr OA Light-On vs 15-hr OA Light-Off;

- Video S1: Representative recordings depicting spontaneous calcium activity in neurons cultured on different substrates at Day 14.

falahatdoost_supplement.pdf

Video S1. Calcium Imaging.mp4

AUTHOR INFORMATION

Corresponding Author

*wei.tong@unimelb.edu.au

Author Contributions

The manuscript was written through contributions of all authors. All authors have given approval to the final version of the manuscript.

Funding sources

This research was funded by a Medicine/Science Grant from the CASS Foundation (CASS 8612), a Linkage Grant from the Australian Research Council (LP180100638) and a grant from the Australian College of Optometry. MBC was supported by National Health and Medical Research Council (APP11968410). WT was supported by a University of Melbourne Early Career Researcher Grant (2021ECR091) and a Discovery Early Career Researcher Award (DECRA) Fellowship from The Australian Research Council (DE220100302).

Declaration of competing interest

SP was previously a shareholder in iBIONICS, a company developing a diamond-based retinal implant. SP, DJG and MRI are shareholders and public officers of Carbon Cybernetics Pty Ltd., a company developing diamond and carbon-based medical device components. The remaining authors declare that the research was conducted in the absence of any commercial or financial relationships that could be construed as a potential conflict of interest.

Data availability

Fastq files from RNA sequencing are available from ENA under accession PRJEB65954. Other data can be provided by the authors upon reasonable request.

Acknowledgement

The authors acknowledge the facilities, as well as the scientific and technical assistance of the Australian Microscopy & Microanalysis Research Facility at the RMIT University.

REFERENCES

(1) Chen, R.; Canales, A.; Anikeeva, P. Neural Recording and Modulation Technologies. *Nature Reviews Materials* **2017,** *2* (2), 1-16.

(2) Gelmi, A.; Schutt, C. E. Stimuli-Responsive Biomaterials: Scaffolds for Stem Cell Control. *Advanced Healthcare Materials* **2021,** *10* (1), 2001125.

(3) Willand, M. P.; Nguyen, M.-A.; Borschel, G. H.; Gordon, T. Electrical Stimulation to Promote Peripheral Nerve Regeneration. *Neurorehabilitation and neural repair* **2016,** *30* (5), 490-496.

(4) Zuo, K. J.; Gordon, T.; Chan, K. M.; Borschel, G. H. Electrical Stimulation to Enhance Peripheral Nerve Regeneration: Update in Molecular Investigations and Clinical Translation. *Experimental Neurology* **2020,** *332*, 113397.

(5) Zhao, D.; Huang, R.; Gan, J.-M.; Shen, Q.-D. Photoactive Nanomaterials for Wireless Neural Biomimetics, Stimulation, and Regeneration. *ACS nano* **2022,** *16* (12), 19892-19912.

(6) Lee, H. P.; Gaharwar, A. K. Light-Responsive Inorganic Biomaterials for Biomedical Applications. *Advanced Science* **2020,** *7* (17), 2000863.

(7) Jiang, Y.; Parameswaran, R.; Li, X.; Carvalho-de-Souza, J. L.; Gao, X.; Meng, L.; Bezanilla, F.; Shepherd, G. M.; Tian, B. Nongenetic Optical Neuromodulation with Silicon-Based Materials. *Nature protocols* **2019,** *14* (5), 1339-1376.

(8) Yang, K.; Oh, J. Y.; Lee, J. S.; Jin, Y.; Chang, G.-E.; Chae, S. S.; Cheong, E.; Baik, H. K.; Cho, S.-W. Photoactive Poly (3-Hexylthiophene) Nanoweb for Optoelectrical Stimulation to Enhance Neurogenesis of Human Stem Cells. *Theranostics* **2017,** *7* (18), 4591.
(9) Yuan, B.; Aziz, M. R. F.; Li, S.; Wu, J.; Li, D.; Li, R.-K. An Electro-Spun Tri-Component Polymer Biomaterial with Optoelectronic Properties for Neuronal Differentiation. *Acta Biomaterialia* **2022,** *139*, 82-90.
(10) Wu, Y.; Peng, Y.; Bohra, H.; Zou, J.; Ranjan, V. D.; Zhang, Y.; Zhang, Q.; Wang, M. Photoconductive Micro/Nanoscale Interfaces of a Semiconducting Polymer for Wireless Stimulation of Neuron-Like Cells. *ACS applied materials & interfaces* **2019,** *11* (5), 4833-4841.
(11) Hsiao, Y.-S.; Liao, Y.-H.; Chen, H.-L.; Chen, P.; Chen, F.-C. Organic Photovoltaics and Bioelectrodes Providing Electrical Stimulation for Pc12 Cell Differentiation and Neurite Outgrowth. *ACS applied materials & interfaces* **2016,** *8* (14), 9275-9284.
(12) Milos, F.; Tullii, G.; Gobbo, F.; Lodola, F.; Galeotti, F.; Verpelli, C.; Mayer, D.; Maybeck, V.; Offenhäusser, A.; Antognazza, M. R. High Aspect Ratio and Light-Sensitive Micropillars Based on a Semiconducting Polymer Optically Regulate Neuronal Growth. *ACS Applied Materials & Interfaces* **2021,** *13* (20), 23438-23451.
(13) Onorato, G.; Fardella, F.; Lewinska, A.; Gobbo, F.; Tommasini, G.; Wnuk, M.; Tino, A.; Moros, M.; Antognazza, M. R.; Tortiglione, C. Optical Control of Tissue Regeneration through Photostimulation of Organic Semiconducting Nanoparticles. *Advanced Healthcare Materials* **2022,** *11* (19), 2200366.
(14) Wu, C.; Pu, Y.; Zhang, Y.; Liu, X.; Qiao, Z.; Xin, N.; Zhou, T.; Chen, S.; Zeng, M.; Tang, J. A Bioactive and Photoresponsive Platform for Wireless Electrical Stimulation to Promote Neurogenesis. *Advanced Healthcare Materials* **2022,** *11* (20), 2201255.
(15) Tang, J.; Wu, C.; Qiao, Z.; Pi, J.; Zhang, Y.; Luo, F.; Sun, J.; Wei, D.; Fan, H. A Photoelectric Effect Integrated Scaffold for the Wireless Regulation of Nerve Cellular Behavior. *Journal of Materials Chemistry B* **2022,** *10* (10), 1601-1611.
(16) Maya-Vetencourt, J. F.; Manfredi, G.; Mete, M.; Colombo, E.; Bramini, M.; Di Marco, S.; Shmal, D.; Mantero, G.; Dipalo, M.; Rocchi, A. Subretinally Injected Semiconducting Polymer Nanoparticles Rescue Vision in a Rat Model of Retinal Dystrophy. *Nature nanotechnology* **2020,** *15* (8), 698-708.
(17) Akhavan, O.; Ghaderi, E. Flash Photo Stimulation of Human Neural Stem Cells on Graphene/Tio 2 Heterojunction for Differentiation into Neurons. *Nanoscale* **2013,** *5* (21), 10316-10326.
(18) Akhavan, O.; Ghaderi, E. The Use of Graphene in the Self-Organized Differentiation of Human Neural Stem Cells into Neurons under Pulsed Laser Stimulation. *Journal of Materials Chemistry B* **2014,** *2* (34), 5602-5611.
(19) Akhavan, O.; Ghaderi, E.; Shirazian, S. A. Near Infrared Laser Stimulation of Human Neural Stem Cells into Neurons on Graphene Nanomesh Semiconductors. *Colloids and Surfaces B: Biointerfaces* **2015,** *126*, 313-321.
(20) Zhang, Z.; Xu, R.; Wang, Z.; Dong, M.; Cui, B.; Chen, M. Visible-Light Neural Stimulation on Graphitic-Carbon Nitride/Graphene Photocatalytic Fibers. *ACS applied materials & interfaces* **2017,** *9* (40), 34736-34743.

(21) Zhang, Z.; Jørgensen, M. L.; Wang, Z.; Amagat, J.; Wang, Y.; Li, Q.; Dong, M.; Chen, M. 3d Anisotropic Photocatalytic Architectures as Bioactive Nerve Guidance Conduits for Peripheral Neural Regeneration. *Biomaterials* **2020,** *253*, 120108.
(22) Amagat, J.; Müller, C. A.; Jensen, B. N.; Xiong, X.; Su, Y.; Christensen, N. P.; Le Friec, A.; Dong, M.; Fang, Y.; Chen, M. Injectable 2d Flexible Hydrogel Sheets for Optoelectrical/Biochemical Dual Stimulation of Neurons. *Biomaterials Advances* **2023**, 213284.
(23) Yan, Z.; Li, K.; Shao, D.; Shen, Q.; Ding, Y.; Huang, S.; Xie, Y.; Zheng, X. Visible-Light-Responsive Reduced Graphene Oxide/Gc 3 N 4/Tio 2 Composite Nanocoating for Photoelectric Stimulation of Neuronal and Osteoblastic Differentiation. *RSC advances* **2022,** *12* (15), 8878-8888.
(24) Nistor, P.; May, P. Diamond Thin Films: Giving Biomedical Applications a New Shine. *Journal of the royal society interface* **2017,** *14* (134), 20170382.
(25) Garrett, D. J.; Tong, W.; Simpson, D. A.; Meffin, H. Diamond for Neural Interfacing: A Review. *Carbon* **2016,** *102*, 437-454.
(26) Pandey, P. C.; Shukla, S.; Pandey, G.; Narayan, R. J. Nanostructured Diamond for Biomedical Applications. *Nanotechnology* **2021,** *32* (13), 132001.
(27) Sommer, A. P.; Jaganathan, S.; Maduro, M. R.; Hancke, K.; Janni, W.; Fecht, H.-J. Genesis on Diamonds Ii: Contact with Diamond Enhances Human Sperm Performance by 300%. *Annals of translational medicine* **2016,** *4* (20), 407-412.
(28) May, P. W.; Regan, E. M.; Taylor, A.; Uney, J.; Dick, A. D.; McGeehan, J. Spatially Controlling Neuronal Adhesion on Cvd Diamond. *Diamond and related materials* **2012,** *23*, 100-104.
(29) Taylor, A. C.; Vagaska, B.; Edgington, R.; Hébert, C.; Ferretti, P.; Bergonzo, P.; Jackman, R. B. Biocompatibility of Nanostructured Boron Doped Diamond for the Attachment and Proliferation of Human Neural Stem Cells. *J Neural Eng* **2015,** *12* (6), 066016.
(30) Bhattacharyya, S.; Auciello, O.; Birrell, J.; Carlisle, J.; Curtiss, L.; Goyette, A.; Gruen, D.; Krauss, A.; Schlueter, J.; Sumant, A. Synthesis and Characterization of Highly-Conducting Nitrogen-Doped Ultrananocrystalline Diamond Films. *Applied Physics Letters* **2001,** *79* (10), 1441-1443.
(31) Birrell, J.; Gerbi, J.; Auciello, O.; Gibson, J.; Gruen, D.; Carlisle, J. Bonding Structure in Nitrogen Doped Ultrananocrystalline Diamond. *Journal of Applied Physics* **2003,** *93* (9), 5606-5612.
(32) Tong, W.; Fox, K.; Zamani, A.; Turnley, A. M.; Ganesan, K.; Ahnood, A.; Cicione, R.; Meffin, H.; Prawer, S.; Stacey, A. Optimizing Growth and Post Treatment of Diamond for High Capacitance Neural Interfaces. *Biomaterials* **2016,** *104*, 32-42.
(33) Falahatdoost, S.; Chambers, A.; Stacey, A.; Prawer, S.; Ahnood, A. Towards Optical Neuromodulation Using Nitrogen-Doped Ultrananocrystalline Diamond Photoelectrodes. *Surfaces and Interfaces* **2022,** *30*, 101850.
(34) Chambers, A.; Ahnood, A.; Falahatdoost, S.; Yianni, S.; Hoxley, D.; Johnson, B. C.; Garrett, D. J.; Tomljenovic-Hanic, S.; Prawer, S. Near-Infrared Excitation of Nitrogen-Doped Ultrananocrystalline Diamond Photoelectrodes in Saline Solution. *Diamond and Related Materials* **2020,** *103*, 107720.
(35) Garrett, D. J.; Ganesan, K.; Stacey, A.; Fox, K.; Meffin, H.; Prawer, S. Ultra-Nanocrystalline Diamond Electrodes: Optimization Towards Neural Stimulation Applications. *J Neural Eng* **2012,** *9* (1), DOI: Artn 016002

10.1088/1741-2560/9/1/016002.

(36) Ahnood, A.; Meffin, H.; Garrett, D. J.; Fox, K.; Ganesan, K.; Stacey, A.; Apollo, N. V.; Wong, Y. T.; Lichter, S. G.; Kentler, W. Diamond Devices for High Acuity Prosthetic Vision. *Advanced biosystems* **2017,** *1* (1-2), 1600003.
(37) Garrett, D. J.; Saunders, A. L.; McGowan, C.; Specks, J.; Ganesan, K.; Meffin, H.; Williams, R. A.; Nayagam, D. A. X. In Vivo Biocompatibility of Boron Doped and Nitrogen Included Conductive-Diamond for Use in Medical Implants. *J Biomed Mater Res B* **2016,** *104* (1), 19-26, DOI: 10.1002/jbm.b.33331.
(38) Hejazi, M. A.; Tong, W.; Stacey, A.; Soto-Breceda, A.; Ibbotson, M. R.; Yunzab, M.; Maturana, M. I.; Almasi, A.; Jung, Y. J.; Sun, S. Hybrid Diamond/Carbon Fiber Microelectrodes Enable Multimodal Electrical/Chemical Neural Interfacing. *Biomaterials* **2020,** *230*, 119648.
(39) Tong, W.; Meffin, H.; Garrett, D. J.; Ibbotson, M. R. Stimulation Strategies for Improving the Resolution of Retinal Prostheses. *Frontiers in neuroscience* **2020,** *14*, 262.
(40) Stamp, M. E.; Tong, W.; Ganesan, K.; Prawer, S.; Ibbotson, M. R.; Garrett, D. J. 3d Diamond Electrode Array for High-Acuity Stimulation in Neural Tissue. *ACS Applied Bio Materials* **2020,** *3* (3), 1544-1552.
(41) Hadjinicolaou, A. E.; Leung, R. T.; Garrett, D. J.; Ganesan, K.; Fox, K.; Nayagam, D. A.; Shivdasani, M. N.; Meffin, H.; Ibbotson, M. R.; Prawer, S. Electrical Stimulation of Retinal Ganglion Cells with Diamond and the Development of an All Diamond Retinal Prosthesis. *Biomaterials* **2012,** *33* (24), 5812-5820.
(42) Ganesan, K.; Garrett, D. J.; Ahnood, A.; Shivdasani, M. N.; Tong, W.; Turnley, A. M.; Fox, K.; Meffin, H.; Prawer, S. An All-Diamond, Hermetic Electrical Feedthrough Array for a Retinal Prosthesis. *Biomaterials* **2014,** *35* (3), 908-915.
(43) Ahnood, A.; Simonov, A. N.; Laird, J. S.; Maturana, M. I.; Ganesan, K.; Stacey, A.; Ibbotson, M. R.; Spiccia, L.; Prawer, S. Transient Photoresponse of Nitrogen-Doped Ultrananocrystalline Diamond Electrodes in Saline Solution. *Applied Physics Letters* **2016,** *108* (10), DOI: Artn 104103

10.1063/1.4942976.
(44) Chambers, A.; Prawer, S.; Ahnood, A. Photoelectrochemical Modelling of Semiconducting Electrodes for Neural Interfacing. *Journal of The Electrochemical Society* **2023,** *170* (2), 026502.
(45) Ahnood, A.; Chambers, A.; Gelmi, A.; Yong, K.-T.; Kavehei, O. Semiconducting Electrodes for Neural Interfacing: A Review. *Chemical Society Reviews* **2023**, 1491-1518.
(46) Merrill, D. R.; Bikson, M.; Jefferys, J. G. R. Electrical Stimulation of Excitable Tissue: Design of Efficacious and Safe Protocols. *J Neurosci Meth* **2005,** *141* (2), 171-198, DOI: 10.1016/j.jneumeth.2004.10.020.
(47) Tedford, C. E.; DeLapp, S.; Jacques, S.; Anders, J. Quantitative Analysis of Transcranial and Intraparenchymal Light Penetration in Human Cadaver Brain Tissue. *Lasers in surgery and medicine* **2015,** *47* (4), 312-322.
(48) Green, R. A.; Hassarati, R. T.; Bouchinet, L.; Lee, C. S.; Cheong, G. L. M.; Yu, J. F.; Dodds, C. W.; Suaning, G. J.; Poole-Warren, L. A.; Lovell, N. H. Substrate Dependent Stability of Conducting Polymer Coatings on Medical Electrodes. *Biomaterials* **2012,** *33* (25), 5875-5886, DOI: 10.1016/j.biomaterials.2012.05.017.
(49) Gordon, J.; Amini, S. General Overview of Neuronal Cell Culture. *Neuronal Cell Culture: Methods and Protocols* **2021**, 1-8.

(50) Saha, K.; Keung, A. J.; Irwin, E. F.; Li, Y.; Little, L.; Schaffer, D. V.; Healy, K. E. Substrate Modulus Directs Neural Stem Cell Behavior. *Biophysical journal* **2008,** *95* (9), 4426-4438.
(51) Ge, S. X.; Son, E. W.; Yao, R. Idep: An Integrated Web Application for Differential Expression and Pathway Analysis of Rna-Seq Data. *BMC bioinformatics* **2018,** *19* (1), 1-24.
(52) Kelsell, D. P.; Dunlop, J.; Stevens, H. P.; Lench, N. J.; Liang, J.; Parry, G.; Mueller, R. F.; Leigh, I. M. Connexin 26 Mutations in Hereditary Non-Syndromic Sensorineural Deafness. *Nature* **1997,** *387* (6628), 80-83.
(53) Grifa, A.; Wagner, C. A.; D'Ambrosio, L.; Melchionda, S.; Bernardi, F.; Lopez-Bigas, N.; Rabionet, R.; Arbones, M.; Monica, M. D.; Estivill, X. Mutations in Gjb6 Cause Nonsyndromic Autosomal Dominant Deafness at Dfna3 Locus. *Nature genetics* **1999,** *23* (1), 16-18.
(54) Dong, A.; Liu, S.; Li, Y. Gap Junctions in the Nervous System: Probing Functional Connections Using New Imaging Approaches. *Frontiers in Cellular Neuroscience* **2018,** *12*, 320.
(55) Hirano, S.; Suzuki, S. T.; Redies, C. The Cadherin Superfamily in Neural Development: Diversity, Function and Interaction with Other Molecules. *Frontiers in Bioscience-Landmark* **2003,** *8* (4), 306-355.
(56) SANDBERG-LALL, M.; HÄGG, P. O.; WAHLSTRÖM, I.; PIHLAJANIEMI, T. Type Xiii Collagen Is Widely Expressed in the Adult and Developing Human Eye and Accentuated in the Ciliary Muscle, the Optic Nerve and the Neural Retina. *Experimental eye research* **2000,** *70* (4), 401-410.
(57) Hubert, T.; Grimal, S.; Carroll, P.; Fichard-Carroll, A. Collagens in the Developing and Diseased Nervous System. *Cellular and molecular life sciences* **2009,** *66* (7), 1223-1238.
(58) Amaral, M.; Dias, A.; Gomes, P.; Lopes, M.; Silva, R.; Santos, J.; Fernandes, M. Nanocrystalline Diamond: In Vitro Biocompatibility Assessment by Mg63 and Human Bone Marrow Cells Cultures. *Journal of Biomedical Materials Research Part A: An Official Journal of The Society for Biomaterials, The Japanese Society for Biomaterials, and The Australian Society for Biomaterials and the Korean Society for Biomaterials* **2008,** *87* (1), 91-99.
(59) Lechleitner, T.; Klauser, F.; Seppi, T.; Lechner, J.; Jennings, P.; Perco, P.; Mayer, B.; Steinmüller-Nethl, D.; Preiner, J.; Hinterdorfer, P. The Surface Properties of Nanocrystalline Diamond and Nanoparticulate Diamond Powder and Their Suitability as Cell Growth Support Surfaces. *Biomaterials* **2008,** *29* (32), 4275-4284.
(60) Rezek, B.; Ukraintsev, E.; Krátká, M.; Taylor, A.; Fendrych, F.; Mandys, V. Epithelial Cell Morphology and Adhesion on Diamond Films Deposited and Chemically Modified by Plasma Processes. *Biointerphases* **2014,** *9* (3), 031012.
(61) Chen, Y.-C.; Lee, D.-C.; Hsiao, C.-Y.; Chung, Y.-F.; Chen, H.-C.; Thomas, J. P.; Pong, W.-F.; Tai, N.-H.; Lin, I.-N.; Chiu, M. The Effect of Ultra-Nanocrystalline Diamond Films on the Proliferation and Differentiation of Neural Stem Cells. *Biomaterials* **2009,** *30* (20), 3428-3435.
(62) Hoffman-Kim, D.; Mitchel, J. A.; Bellamkonda, R. V. Topography, Cell Response, and Nerve Regeneration. *Annu Rev Biomed Eng* **2010,** *12*, 203-231, DOI: 10.1146/annurev-bioeng-070909-105351.
(63) Wei, J.; Yoshinari, M.; Takemoto, S.; Hattori, M.; Kawada, E.; Liu, B.; Oda, Y. Adhesion of Mouse Fibroblasts on Hexamethyldisiloxane Surfaces with Wide Range of Wettability. *Journal of Biomedical Materials Research Part B: Applied Biomaterials: An Official Journal of The Society for Biomaterials, The Japanese Society for Biomaterials, and The Australian Society for Biomaterials and the Korean Society for Biomaterials* **2007,** *81* (1), 66-75.

(64) Pereda, A. E.; Curti, S.; Hoge, G.; Cachope, R.; Flores, C. E.; Rash, J. E. Gap Junction-Mediated Electrical Transmission: Regulatory Mechanisms and Plasticity. *Biochimica et Biophysica Acta (BBA)-Biomembranes* **2013,** *1828* (1), 134-146.
(65) Hamblin, M. R. Shining Light on the Head: Photobiomodulation for Brain Disorders. *BBA clinical* **2016,** *6*, 113-124.
(66) Merrill, D. R.; Bikson, M.; Jefferys, J. G. Electrical Stimulation of Excitable Tissue: Design of Efficacious and Safe Protocols. *J Neurosci Meth* **2005,** *141* (2), 171-198.
(67) Liu, Z. G.; Dong, L. Q.; Cheng, K.; Luo, Z. K.; Weng, W. J. Charge Injection Based Electrical Stimulation on Polypyrrole Planar Electrodes to Regulate Cellular Osteogenic Differentiation. *Rsc Advances* **2018,** *8* (33), 18470-18479, DOI: 10.1039/c8ra02601g.
(68) Schindelin, J.; Arganda-Carreras, I.; Frise, E.; Kaynig, V.; Longair, M.; Pietzsch, T.; Preibisch, S.; Rueden, C.; Saalfeld, S.; Schmid, B.; Tinevez, J. Y.; White, D. J.; Hartenstein, V.; Eliceiri, K.; Tomancak, P.; Cardona, A. Fiji: An Open-Source Platform for Biological-Image Analysis. *Nat Methods* **2012,** *9* (7), 676-682, DOI: 10.1038/Nmeth.2019.
(69) Radstake, F. D. W.; Raaijmakers, E. A. L.; Luttge, R.; Zinger, S.; Frimat, J. P. Calima: The Semi-Automated Open-Source Calcium Imaging Analyzer. *Comput Meth Prog Bio* **2019,** *179*, DOI: ARTN 104991

10.1016/j.cmpb.2019.104991.
(70) Dobin, A.; Davis, C. A.; Schlesinger, F.; Drenkow, J.; Zaleski, C.; Jha, S.; Batut, P.; Chaisson, M.; Gingeras, T. R. Star: Ultrafast Universal Rna-Seq Aligner. *Bioinformatics* **2013,** *29* (1), 15-21.

For Table of Contents Only